

MAARS: a novel high-content acquisition software for the analysis of mitotic defects in fission yeast

Tong Li, Hadrien Mary, Marie Grosjean, Jonathan Fouchard, Simon Cabello, Céline Reyes, Sylvie Tournier*, and Yannick Gachet*

Laboratoire de Biologie Cellulaire et Moléculaire du Contrôle de la Prolifération, Centre de Biologie Intégrative, Université de Toulouse, CNRS, UPS, 31062 Toulouse Cedex, France

ABSTRACT Faithful segregation of chromosomes during cell division relies on multiple processes such as chromosome attachment and correct spindle positioning. Yet mitotic progression is defined by multiple parameters, which need to be quantitatively evaluated. To study the spatiotemporal control of mitotic progression, we developed a high-content analysis (HCA) approach that combines automated fluorescence microscopy with real-time quantitative image analysis and allows the unbiased acquisition of multiparametric data at the single-cell level for hundreds of cells simultaneously. The Mitotic Analysis and Recording System (MAARS) provides automatic and quantitative single-cell analysis of mitotic progression on an open-source platform. It can be used to analyze specific characteristics such as cell shape, cell size, metaphase/anaphase delays, and mitotic abnormalities including spindle mispositioning, spindle elongation defects, and chromosome segregation defects. Using this HCA approach, we were able to visualize rare and unexpected events of error correction during anaphase in wild-type or mutant cells. Our study illustrates that such an expert system of mitotic progression is able to highlight the complexity of the mechanisms required to prevent chromosome loss during cell division.

Monitoring Editor

Kerry S. Bloom
University of North Carolina

Received: Oct 19, 2016

Revised: Mar 14, 2017

Accepted: Apr 20, 2017

INTRODUCTION

The correct partitioning of replicated chromosomes between two daughter cells at each division is essential to prevent genome instability. When this process is perturbed, aneuploid daughter cells (i.e., cells possessing an incorrect chromosome number) are generated. Aneuploidy is a well-known cause of severe genetic diseases, such as Down's syndrome, and is an almost ubiquitous feature of human cancers (Holland and Cleveland, 2009; Compton, 2011). The two

best-known mechanisms leading to aneuploidy involve chromosome segregation and spindle-positioning defects. Abnormal chromosome segregation is caused by defects in surveillance mechanisms (spindle assembly checkpoint or Aurora B kinase) or linked to increased centrosome copy number, kinetochore–microtubule attachment errors, or cell-cycle regulation defects (Vitre and Cleveland, 2012). On the other hand, the control of spindle positioning requires extranuclear players because many cell types orient their spindles according to preexisting polarity cues and use an astral microtubule contact with the cell cortex to position or align the mitotic apparatus (Carminati and Stearns, 1997; Shaw *et al.*, 1997; Adames and Cooper, 2000; Yeh *et al.*, 2000; Gachet *et al.*, 2004; Kozłowski *et al.*, 2007; Kotak and Gonczy, 2013). In addition, chromosome segregation, spindle positioning, and cytokinesis must be coordinated to prevent chromosome loss. Thus multiple mitotic parameters contribute to the spatiotemporal control of chromosome partitioning.

Studies in yeast have contributed to our present understanding of the general principles underlying the regulation of chromosome segregation and spindle positioning in dividing cells (Nurse and Thuriaux, 1980; Page and Snyder, 1993; Yanagida, 1998; Segal and

This article was published online ahead of print in MBoC in Press (<http://www.molbiolcell.org/cgi/doi/10.1091/mbc.E16-10-0723>) on April 27, 2017.

The authors declare no competing interests.

*Address correspondence to: Sylvie Tournier (sylvie.tournier-gachet@univ-tlse3.fr), Yannick Gachet (yannick.gachet@univ-tlse3.fr).

Abbreviations used: CFP, cyan fluorescent protein; DAPI, 4',6-diamidino-2-phenylindole; GFP, green fluorescent protein; HCA, high-content analysis; LoG, Laplacian of Gaussian; M phase, mitotic phase; NA, numerical aperture; PBS, phosphate-buffered saline; RFP, red fluorescent protein; ROI, region of interest; SAC, spindle assembly checkpoint; SPB, spindle pole body; W/L, width to length.

© 2017 Li *et al.* This article is distributed by The American Society for Cell Biology under license from the author(s). Two months after publication it is available to the public under an Attribution–Noncommercial–Share Alike 3.0 Unported Creative Commons License (<http://creativecommons.org/licenses/by-nc-sa/3.0>).

"ASCB®," "The American Society for Cell Biology®," and "Molecular Biology of the Cell®" are registered trademarks of The American Society for Cell Biology.

Bloom, 2001). The fission yeast *Schizosaccharomyces pombe* is a rod-shaped, symmetrically dividing eukaryote that splits by medial fission. *S. pombe* possesses three chromosomes (Kohli *et al.*, 1977), which can be tracked by live imaging during mitotic progression (Tournier *et al.*, 2004). In this organism, mitosis is divided into three phases (Nabeshima *et al.*, 1998; Tatebe *et al.*, 2001), and spindle formation begins in M phase, as in higher eukaryotic cells (Russell *et al.*, 1989). During phase 1 (prophase), a short spindle of $<2.0\ \mu\text{m}$ is formed, and chromosomes are captured by microtubules at kinetochores, large protein complexes assembled at the centromeres of each chromosome. Kinetochores begin to align at the spindle center in phase 1 (Mary *et al.*, 2015). In phase 2 (prometaphase/metaphase/anaphase A), the spindle maintains roughly the same length, and the kinetochores oscillate between the two spindle pole bodies (SPBs; Mary *et al.*, 2015). At the end of phase 2, sister chromatids separate through the activity of an enzyme called separase, which degrades the cohesin link between sister chromatids, allowing their movement toward the SPBs (anaphase A; Yanagida, 2000). At this stage, it is generally accepted that the abrupt change in the rate of spindle elongation signals the beginning of anaphase B (phase 3; Nabeshima *et al.*, 1998). Finally, during cytokinesis, the actomyosin ring contraction initiates the separation of the two daughter cells (Chang and Nurse, 1993).

Chromosome attachment to the mitotic spindle results from a stochastic search-and-capture process that is intrinsically prone to errors (Kirschner and Mitchison, 1986). In *S. pombe*, chromosome capture and biorientation successfully occur within minutes before sister chromatid separation (Grishchuk and McIntosh, 2006; Gachet *et al.*, 2008). This process is particularly efficient due to the presence of surveillance mechanisms that prevent chromosome loss (less than one chromosome is lost in 10^4 divisions). This control is ensured by an error detection and correction system, which involves the Aurora B kinase, a master regulator of cell division (Petersen *et al.*, 2001; Petersen and Hagan, 2003; Sampath *et al.*, 2004; Kotwaliwale *et al.*, 2007; Mora-Bermudez *et al.*, 2007; Steigemann *et al.*, 2009; Tada *et al.*, 2011) and the spindle assembly checkpoint (SAC), which delays anaphase onset in the presence of unattached chromosomes (Rieder *et al.*, 1995; Rudner and Murray, 1996; Cleveland *et al.*, 2003). Aurora B and SAC components operate at the level of kinetochores, where they promote the stabilization of proper attachment and the destabilization of erroneous ones. Of note, in metaphase, Aurora B destabilizes faulty kinetochore-to-microtubule attachments such as merotelic (one chromosome attached to both poles) through the phosphorylation of key kinetochore substrates (Tanaka *et al.*, 2002; Cimini *et al.*, 2006). Merotelic attachment is also corrected after anaphase onset through spindle elongation forces (Courtheoux *et al.*, 2009; Gay *et al.*, 2012). Further work also suggests that metaphase spindle forces are also important to prevent the appearance of lagging chromosomes in anaphase (Choi and McCollum, 2012).

Quantitative analysis of mitotic fidelity in fission yeast is usually addressed using minichromosome-loss experiments (Niwa, 2016). However, this technique cannot be used to determine the precise cause of chromosome loss, and because the rate of chromosome loss is generally very low, the direct cytological examination of chromosome segregation errors using live-cell imaging is not feasible. Thus, to understand fully the mechanisms ensuring the accuracy of mitotic progression, we developed a high-content analysis approach, which combines automated fluorescence microscopy with quantitative image analysis of mitosis. This methodology allows the acquisition of unbiased multiparametric data at the single-cell level for hundreds of cells simultaneously. Although a number of tools

were commercially available (e.g., Operetta High-Content imaging system), as well as open-source tools such as MicroPilot (Conrad *et al.*, 2011), the existing software did not meet our requirement in term of flexibility (use of ImageJ collection of plug-ins) or analysis specificity (measurement of chromosome segregation errors). On the concept of basic machine learning method (i.e., decision tree), we developed automated open-source software called the Mitotic Analysis and Recording System (MAARS). MAARS provides automatic, multiparametric, and quantitative single-cell analysis of mitotic progression. We tested the robustness of this method on several *S. pombe* mutants and were able to identify unexpected phenotypes in wild-type and mutant cells. Our study illustrates the impressive benefits of using MAARS to analyze quantitatively mitotic fidelity in eukaryotic cells.

RESULTS

MAARS: an automated, robust, and open-source software for high-content analysis of mitosis

To analyze quantitatively the mechanisms controlling mitotic fidelity, we developed an automated open-source image acquisition and on-the-fly analysis pipeline named MAARS. We first built the connection between the computer and the microscope using open-source software called Micro-Manager (Edelstein *et al.*, 2010). In contrast to all available commercial software, Micro-Manager supports multiple microscopy platforms and is compatible with the image-processing package ImageJ. Thus MAARS can also be installed on a variety of wide-field microscopes. MAARS delivers a graphic interface and controls image acquisitions via Micro-Manager. With its user-friendly window, it is possible to adjust microscope parameters such as exposure time, frequency of image acquisition, type of color channel, and so on. In addition, specific parameters for mitotic analysis (i.e., size of the spots, type of fluorescent markers) are also selected at this step.

We next implemented an accurate segmentation method to detect fission yeast or budding yeast cells (Figure 1 and Supplemental Figures S1 and S2). This segmentation technique is based on a mathematic algorithm (Julou *et al.*, 2013) that requires only bright field with multiple z-section acquisition (~34 frames) to compute the correlation between cell edges (Supplemental Figure S1B, blue dots) and theoretical cell edges (Supplemental Figure S1B, green curve). Alternative methods consist of marking cell edges (Schmitter *et al.*, 2013) or increasing the contrast between the cell and the background using fluorescent agents (Peng *et al.*, 2013). However, our segmentation technique can be used on nonfluorescent native cell lines with no risk of phototoxicity (Supplemental Figure S1). The cell edges are drawn at the point of high correlation score using Otsu thresholding, as available in ImageJ (Supplemental Figure S1, A–C). Owing to the optimized parallelization described in *Materials and Methods*, MAARS can perform fast segmentation. The acquisition and segmentation of a single field of cells with multiple z-sections takes ~15 s (1100 cells/field; see *Materials and Methods*).

To prevent the segmentation of false-positive cells, we implemented two types of filters—solidity and gray-level filters. The solidity value (area of an object divided by its convex area; Figure 1, bottom) can be adjusted to fit with several cell shapes (round, bent, or long cells). For example, the solidity parameter is 0.84 for *S. pombe* and 0.5 for *Saccharomyces cerevisiae*, as shown in Supplemental Figure S1E. In addition to this cell shape parameter, we implemented a second filter, called gray intensity filter, based on the pixel intensity of the inner cell on correlation image (see *Materials and Methods*. The pixel intensity of the cell is compared directly with the intercell space background; Supplemental Figure S1C). In

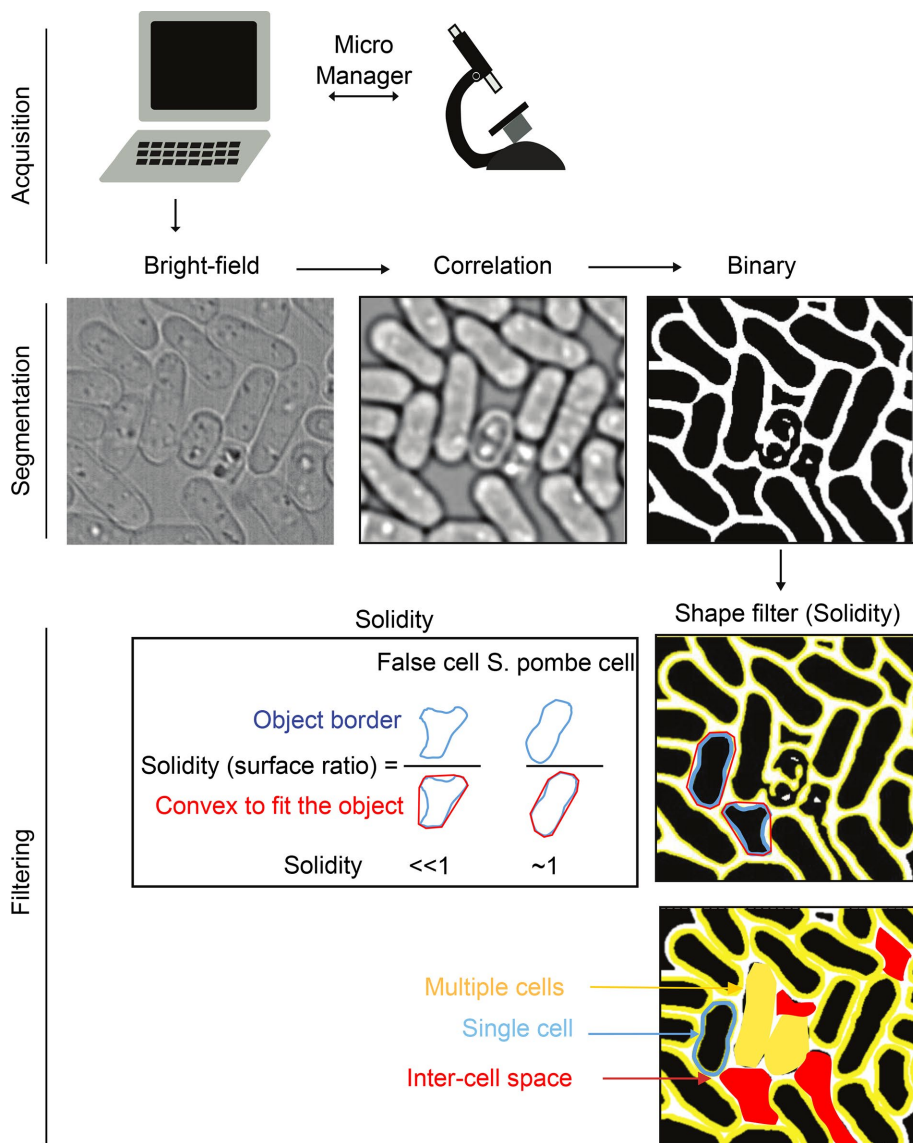


FIGURE 1: The MAARS cell segmentation pipeline. MAARS is a Micro-Manager plug-in that controls the microscope in real time. After acquisition, *S. pombe* segmentation is performed using a correlation imaging technique based on bright-field images taken at various focal positions. Solidity filters (shape and gray filters) are applied to reduce the detection of false positives during segmentation.

the absence of filters, MAARS can detect ~85% of cells per field (Supplemental Figure S1D). The rejected 15% of cells includes cells located on the edge of the image or overlapping cells. Using proper gray filter intensity and solidity, only 1% of the cells ($n = 7434$) were false positives (Supplemental Figure S1D).

After segmentation, fluorescent images are automatically analyzed on the fly with MAARS (Figure 2A and Supplemental Figure S3). Cells are illuminated with the appropriate channel, and fluorescent spots (e.g., spindle poles in cyan fluorescent protein [CFP] or kinetochores in green fluorescent protein [GFP]) are detected using TrackMate (Tinevez *et al.*, 2017). MAARS (Kernel in Java) first determines whether the fluorescent spots are within the cell (Figure 2A and Supplemental Figure S3) before analyzing their position (Figure 2B and Supplemental Figure S3). The recognition of mitotic cells is achieved in several postanalysis steps (extension in Python). MAARS detects cells with two spindle poles that move apart for at least

3 min (spindle elongation). In contrast, when the distance between spindle poles remains constant, the cell is judged to be in telophase/cytokinesis. MAARS classifies cells in metaphase or anaphase as judged by the spindle elongation rates (Figure 2B and Supplemental Figures S3 and S4). Finally, MAARS identifies whether kinetochores (GFP signals) are detected using a line-scan function drawn between the two poles. If a kinetochore is located between the poles after anaphase onset, it is classified as a lagging kinetochore.

MAARS is very efficient because it can detect ~100 mitotic cells per field containing ~1000 unsynchronized cells, and it enables easy retrieval of the films and analyses of interest. To test the performance of MAARS software, we performed high-content acquisition of spindle elongation (spindle pole–spindle pole distance), cell shape, spindle orientation/positioning, rate of spindle elongation, and presence of lagging chromosomes in different genetic backgrounds.

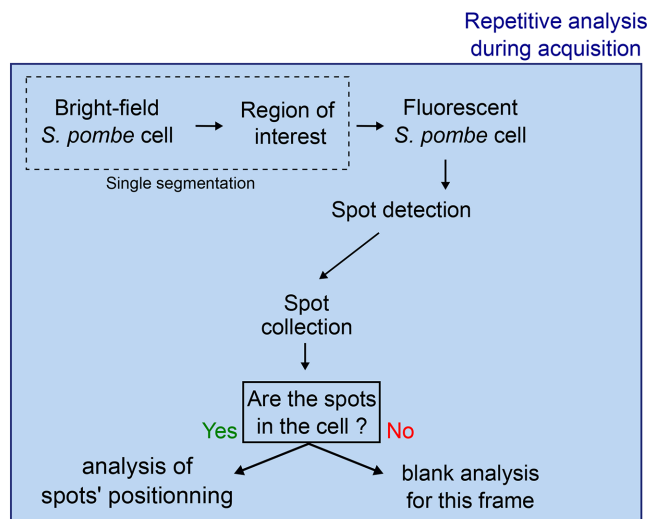
Quantitative analysis of spindle elongation and cell shape distribution to identify cell cycle delays

To evaluate MAARS pipeline, we analyzed several *S. pombe* strains with established cell cycle deficiencies and compared them with wild-type cells. We hypothesized that the distribution of spindle length and cell shape in a population of cells could reveal abnormal cell cycle progression, such as G2 delays or mitotic delays. We chose to measure pole-to-pole distance as an approximation for spindle length because in most situations, spindles are not curved before telophase. *S. pombe* growth occurs during G2, and the integrity of the genome is controlled at this stage before mitotic entry. In the presence of DNA damage or unreplicated DNA, cells are delayed in G2 and become elongated compared with

wild type. Thus cell shape measurement can serve as a good marker to investigate cell cycle defects such as G2 delays. We decided to determine the ratio of width to length (W/L) as a characteristic of cell shape. Long cells (cells delayed in G2: W/L small) are characterized with a very low ratio of vertical axis to longitudinal axis (Figure 3A). In contrast, short cells (short G2 cells: W/L high) are characterized by a high ratio (Figure 3A). For example, in *S. pombe*, cell cycle-deficient cells, also known as *cdc* mutants (Nurse and Thuriaux, 1980), display a G2 cell cycle delay and become elongated before entering mitosis compared with wild-type cells (Figure 3A). We also compared spindle size in *cdc25-22* mutants (Figure 3B, red) versus wild type (Figure 3B, black). MAARS detected two main populations of spindle sizes corresponding to metaphase (maximum peak ~2–3 μm) and anaphase (maximum peak ~6–9 μm ; Figure 3B). As expected, the size of metaphase spindles in the *cdc25-22* mutant was comparable to that in the

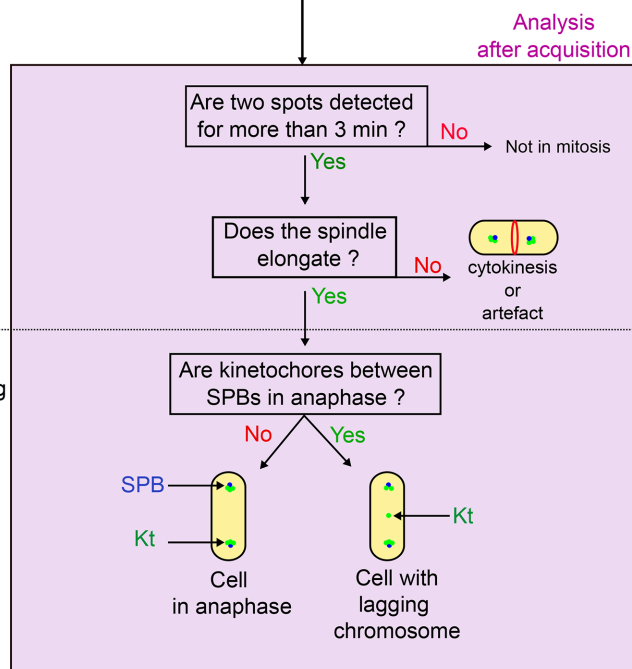
A

MAARS Cell detection and recording



B

MAARS mitotic cell detection



MAARS extension Chromosome lagging detection

FIGURE 2: The MAARS pipeline for the multiparametric analysis of mitosis. (A) MAARS pipeline procedure for cell detection and recording. Cell segmentation is performed only once, and fluorescence signal acquisition is repeated over time. (B) MAARS pipeline procedure for the postacquisition analysis of mitosis (spindle elongation, presence of lagging kinetochores).

wild type, whereas the size of anaphase spindles was larger than that in the wild type (Figure 3B).

We performed a similar analysis in a mutant deficient in kinetochore–microtubule attachment (*mal3Δ*; homologue of EB1 in human; Beinhauer *et al.*, 1997) and in a mutant deficient for the nucleation of cytoplasmic microtubules (*mod20Δ*; Sawin *et al.*, 2004). In the absence of Mal3 and Mod20, we expected a metaphase delay (Zimmerman and Chang, 2005; Asakawa *et al.*, 2006). To test this hypothesis, we analyzed the distribution of spindle size in these mutants and found an accumulation of cells with short spindles (~2–3 μm; Figure 3B, green and blue), suggesting that these proteins were indeed required for normal mitotic progression. In addition, we found that cell shape was modified in these mutants as previously suggested (Beinhauer *et al.*, 1997; Venkatram *et al.*, 2005; Figure 3A,

blue and green). Thus alterations in cell shape or spindle size can be easily quantified using MAARS.

Quantitative analysis of spindle orientation and positioning during mitotic progression

The control of spindle positioning according to the cell center during mitosis is important to prevent anucleated cells. During G2, interphasic microtubules are required to maintain the nucleus at the cell center (Tran *et al.*, 2001), ensuring correct spindle positioning at the beginning of mitosis. To confirm the robustness of MAARS pipeline, we analyzed spindle orientation and positioning during mitotic progression in a population of synchronized cells. A *cdc25-22* thermosensitive mutant expressing SPB markers was blocked for 4 h at 36°C (G2 block) and released synchronously into mitosis at the permissive temperature of 25°C. Mitotic progression was recorded in fixed cells by following the presence of anaphase cells (4',6-diamidino-2-phenylindole [DAPI] staining) or septated cells, characteristic of cytokinesis (calcofluor staining; Figure 4A). In parallel, live-cell analysis using MAARS was conducted every 20 min to analyze the distance between SPBs during mitotic progression (Figure 4B). As expected, we observed an increase in spindle length corresponding to anaphase and telophase cells (Figure 4, B and C). A virtual cell representation shows the average position and length of the spindle (pole-to-pole distance) in this synchronized population of cells (Figure 4D). Combining histograms of pole-to-pole distance, orientation, and positioning as a virtual cell representation proves once again that our analysis pipeline is powerful. We next performed a similar type of experiment to analyze spindle orientation as a function of spindle length (pole-to-pole distance; Figure 4E). In exponentially growing wild-type or *cdc25-22* cells, changes in spindle angle are observed from metaphase to anaphase onset (from 2 to 5 μm). The angle

remains low throughout anaphase B. In contrast and as previously reported, an increased number of cells with misoriented spindles is observed in *mal3Δ* or *mod20Δ* cells from the onset to the end of mitosis (Figure 4E). Our data suggest that the MAARS pipeline is sufficiently sensitive and robust to investigate the mechanisms controlling spindle positioning in a single- or whole-cell population.

Quantitative analysis of spindle elongation during mitotic progression

At the metaphase-to-anaphase transition, an abrupt change in the rate of spindle elongation is observed in fission yeast cells. This change in the slope of the curve can be used as a tool to automatically predict the timing of anaphase and analyze the distribution in spindle elongation rates in single-cell analysis (see *Materials and*

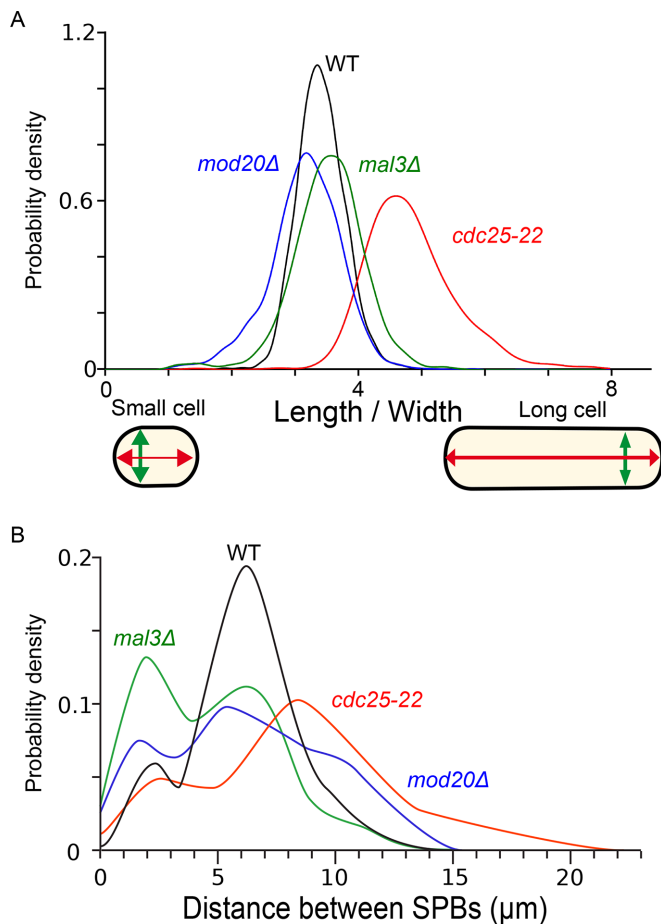


FIGURE 3: Automated analysis of cell shape and pole-to-pole distance distribution in several genetic backgrounds. (A) Normalized density profiles of cell shape in wild-type (black), *cdc25-22* (red), *mal3Δ* (green), and *mod20Δ* (blue) cells. (B) Normalized density profiles of distance between SPBs in wild-type (black), *cdc25-22* (red), *mal3Δ* (green), and *mod20Δ* (blue) cells.

Methods and Supplemental Figure S4). With this method, we analyzed quantitatively the rate of spindle elongation in wild-type (Figure 5A) and mutant cells (Figure 5, B–D) expressing Cdc11-cfp (poles) and Ndc80-GFP (kinetochores; Figure 5, top). To automatically detect anaphase onset, we initially considered looking at colocalization of kinetochores and SPB fluorescence. However, this could not accurately detect anaphase onset in cells defective for the poleward movement of kinetochores at anaphase, as previously observed in the absence of Dam1 (Gao et al., 2010). We thus chose to use the slope-change method, which requires acquisition of a single fluorescent channel, allowing higher-frequency imaging and less photobleaching. Based on spindle elongation slope changes, the MAARS pipeline automatically detected anaphase onset in single cells (time zero in Figure 5, bottom, corresponds to the onset of anaphase, and all the curves are aligned according to time zero). We checked the robustness of this automatic detection of anaphase by directly visualizing kinetochore dynamics in each film (*ndc80-GFP* signal in green). We accurately detected anaphase B onset in 81% ($n = 75$) of analyzed cells. The incorrect detection can be explained by low sample quality (i.e., one SPB moves out of focus during acquisition or either metaphase or anaphase length is too short). This quantitative analysis reveals some heterogeneity in metaphase length in *mal3Δ* (Figure 5C, from -20 to 0 min) and in the cohesin

mutant *rad21-K1* (Figure 5B, from -27 to 0 min) as opposed to wild type (Figure 5A, from -15 to 0 min). Our automated analysis also shows some heterogeneity in spindle elongation rates at anaphase, especially in the case of *rad21-K1* mutant (Figure 5B, bottom), possibly due to the presence of merotelic attachment, as previously reported (Courtheoux et al., 2009).

Thus MAARS provides an efficient tool to analyze spindle elongation and to highlight metaphase delays in individual cells within a population.

Quantitative detection and phenotypic analysis of lagging chromosomes in anaphase

The fidelity of chromosome attachment is ensured by an error detection and correction system that operates in metaphase. However, merotelic attachment can also be corrected at anaphase through spindle elongation forces, and the presence of merotelic attachment in anaphase antagonizes spindle elongation rate (Courtheoux et al., 2009). Thus simultaneous detection of lagging chromosomes with the analysis of spindle elongation in single cells may provide a valuable tool to predict merotelic attachment and follow its correction in live cells.

A frequency analysis of spindle elongation rate in various mutants revealed the presence of two distinct peaks, one corresponding to prophase/metaphase (Figure 6A) and the second to anaphase cells (Figure 6B). From prophase to metaphase, the average rate of spindle elongation was similar between mutants and wild-type cells (-0.1815 $\mu\text{m}/\text{min}$ in wild type; $n = 75$). In contrast, in anaphase, *mod20Δ* and *rad21-K1* mutants exhibited shifted or non-Gaussian distributions of spindle elongation rates compared with wild type (either lower or higher than wild type), although the average elongation rate was similar to wild type (0.7936 $\mu\text{m}/\text{min}$ in wild type, $n = 75$; 0.7950 $\mu\text{m}/\text{min}$ in *mod20Δ*, $n = 33$; and 0.8241 $\mu\text{m}/\text{min}$ in *rad21-K1*, $n = 88$). To test whether some of these defects could be attributed to merotelic attachment, we upgraded the MAARS pipeline with a Python extension to automatically detect the presence of lagging kinetochores at anaphase in cells expressing spindle poles and kinetochore markers (see Materials and Methods and Supplemental Figure S3). The analysis of the films revealed several types of phenotypes. The cohesin mutant *rad21-K1* displayed a large number of single, stretched kinetochores during anaphase (Figure 6, C and D; $14.45\% \pm 4.67$; three independent experiments performed for a total number of mitoses of 254; Supplemental Movie S1), coinciding with changes in the rate of spindle elongation (Figure 6E, yellow) compared with *rad21-K1* cells without lagging kinetochores (Figure 6E, pink). These stretched lagging kinetochores were not observed in wild type (Figure 6F, yellow; $n = 187$) or *mal3Δ* cells (Figure 6F, yellow; $n = 203$) and only occasionally detected in *mod20Δ* cells (Figure 6F, yellow; $2.02\% \pm 1.58$; three independent experiments performed for a total number of mitoses of 148). In wild-type and mutant cells, we also recorded the presence of unstretched lagging kinetochores (Figure 6F, red; defined as a lagging kinetochore that regain the poles 40 s to 1 min later than other kinetochores). This type of lagging kinetochore did not affect the rate of spindle elongation (unpublished data). These results prompted us to perform a quantitative analysis of kinetochore segregation in wild-type cells to evaluate the efficiency of correction mechanisms in wild-type background. We extensively filmed wild-type cells ($n > 8000$) expressing spindle pole and kinetochore markers and identified the presence of two additional types of error correction. In the first type, a pair of kinetochores (as opposed to a single chromatid) separated later than the other pairs but regained the poles soon after (Supplemental Figure S5, a single event in >8000 mitotic cells; and Supplemental Movie S2),

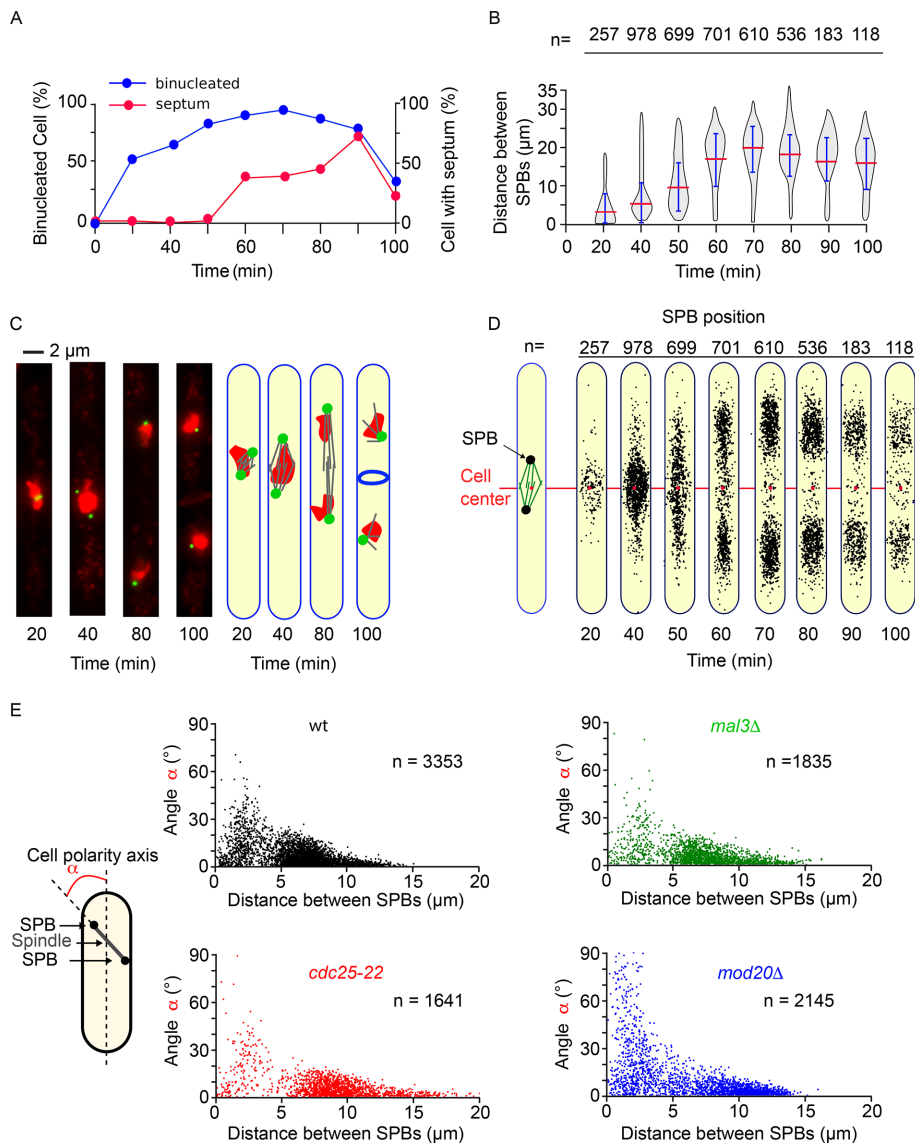


FIGURE 4: Automated analysis of spindle positioning in several genetic backgrounds. (A) Percentage of binucleated cells (blue) and septated cells (red) during *cdc25-22* block and release at 25°C. (B) Violin plots of the pole-to-pole distances during *cdc25-22* block and release at 25°C. Error bars corresponds to SDs. (C) Representative images of *cdc25-22* cells after release at 25°C. The SPBs are in green (Cdc11-GFP), and the nucleus is in red (DAPI). (D) Virtual cell representation showing SPB position in the synchronized population of *cdc25-22* cells in A and B. (E) Analysis of spindle angle according to the distance between SPBs in exponentially growing wild-type (black), *cdc25-22* (red), *mal3Δ* (green), and *mod20Δ* (blue) cells.

suggesting that in some circumstances, cohesin is not degraded uniformly on all chromosomes. In the second type, we observed the correction of a missegregated chromatid after anaphase B onset (i.e., the missegregated chromatid eventually moved from the wrong pole to the correct one; Figure 7, A and B, one event for >8000 mitotic cells; Supplemental Movie S3), suggesting that correction of misattachment does not occur only during metaphase.

In conclusion, our study illustrates the power of MAARS software to identify new and rare events of chromosome segregation defects in wild-type or mutant conditions.

DISCUSSION

In this study, we developed an expert system to automatically analyze mitotic progression. As illustrated in the video tutorial

(<https://github.com/bnoi/MAARS/tree/master/doc/demos>), our software is able to record cell division, specifically find mitotic cells, and extract on-the-fly multiple mitotic parameters. Our results demonstrate that MAARS is practical, time-efficient, and robust software for the multiparametric analysis of mitosis. This software provides statistical analysis at the cell population or single-cell level. Within the entire cell population, MAARS determines the percentage of cells in metaphase, anaphase, or cytokinesis and identifies cell size, spindle pole position, and so on. The results are displayed as a spots distribution, but it is possible to return to the cell image to confirm unexpected results. MAARS can adapt to different cell types (including the budding yeast by adjusting the solidity parameter) and different fluorescent markers (GFP, red fluorescent protein [RFP], or CFP). By simply adjusting the solidity parameter, it is possible to use MAARS for the analysis of cells displaying abnormal cell shapes, such as a pear or T shape. We tested MAARS with long cells (*cdc25-22*) and short cells (*wee1-50*; Nurse, 1975) and obtained very similar data qualities, suggesting that our software is insensitive to cell shape variations (unpublished data).

In this study, we specifically used MAARS to detect spindle poles and kinetochores, but other types of organelles could be detected by simply adjusting MAARS parameters such as number, size, or shape of spots. Of importance, MAARS is delivered with the software Micro-Manager and is freely available (Edelstein et al., 2010). By characterizing a population of 10,000 cells within 5 min, MAARS provides statistical significance comparable to flow cytometry combined with a spatiotemporal analysis of mitotic events. MAARS can extract several parameters from single cells, such as spindle size, orientation, positioning, and elongation, as well as mitotic phase duration. MAARS was tested in various conditions and challenged with established genetic mutants. Our

quantitative single-cell analysis revealed an unexpected heterogeneity in cell size, spindle elongation rate, and spindle positioning in *mal3Δ* or *mod20Δ* mutants, which are defective for cytoplasmic microtubule dynamics. Of importance, most of these differences were not detected when average values were measured. These observations illustrate the strength of using MAARS for quantitative analysis of mitosis as opposed to a classic manual phenotypic analysis.

In addition to these mitotic parameters, MAARS can also detect automatically the presence of unattached kinetochores (kinetochores that are not present on a line drawn between the two SPBs; unpublished data). This may be extremely useful for studying the mechanisms of kinetochore retrieval in fission yeast (Grishchuk and McIntosh, 2006; Franco et al., 2007; Gachet et al., 2008; Kalinina et al., 2013). Another important defect occurring in mitosis is the

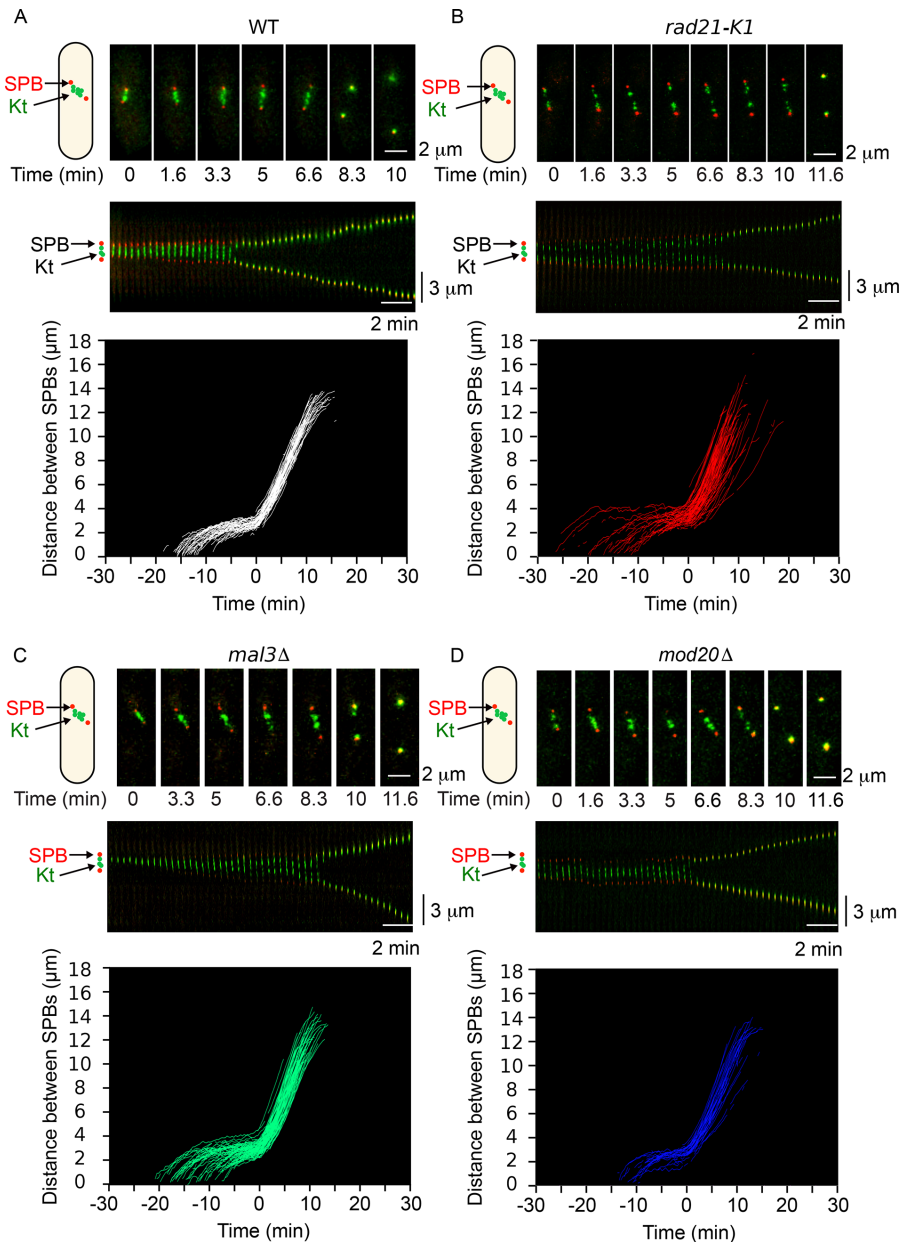


FIGURE 5: Automated analysis of spindle elongation and anaphase B onset in several genetic backgrounds. (A) Top, representative single-cell analysis of mitotic progression in a wild-type cell showing the SPBs (red) and the kinetochores (green). Middle, kymograph representation of mitotic progression of the cell shown above. Bottom, profile of spindle elongation in wild-type cells (white; $n = 75$). Time zero corresponds to anaphase B onset. (B) Top, representative single-cell analysis of mitotic progression in a *rad21-K1* mutant showing the SPBs (red) and the kinetochores (green). Middle, kymograph representation of mitotic progression of the cell shown above. Bottom, profile of spindle elongation in *rad21-K1* mutant (green; $n = 88$). Time zero corresponds to anaphase B onset. (C) Top, representative single cell analysis of mitotic progression in a *mal3Δ* mutant, showing the SPBs (red) and the kinetochores (green). Middle, kymograph representation of mitotic progression of the cell shown above. Bottom, profile of spindle elongation in *mal3Δ* mutant (blue; $n = 92$). Time zero corresponds to anaphase B onset. (D) Top, representative single-cell analysis of mitotic progression in a *mod20Δ* mutant showing SPBs (red) and kinetochores (green). Middle, kymograph representation of mitotic progression of the cell shown above. Bottom, profile of spindle elongation in *mod20Δ* mutant (red; $n = 33$). Time zero corresponds to anaphase B onset.

appearance of a monopolar spindle, which corresponds to defects in spindle formation (Vardy and Toda, 2000). MAARS can also detect this type of defect as long as SPBs are duplicated and detected as

we will be able to detect and analyze prokaryotic cell division with either single or multiple chromosomes. In the future, it will even be possible to analyze metazoan mitotic progression using spindle poles

two distinct spots. Finally, MAARS automatically detects the presence of lagging chromosomes, including stretched merotelic attachment during mitotic progression. Merotelic attachment is the most frequent error during metaphase in eukaryotic cells. Several studies reported the presence of merotelic attachment in mammalian cells released from nocodazole treatment (Cimini *et al.*, 2004) or in *S. pombe* cohesin mutants (Gregan *et al.*, 2007; Courtheoux *et al.*, 2009; Rumpf *et al.*, 2010), although this attachment defect has not been observed in wild-type conditions. Merotelic attachment leads to intrakinetochores stretching followed by correction in anaphase through spindle elongation mechanical forces (Cimini *et al.*, 2004; Courtheoux *et al.*, 2009). Of note, the presence of merotelic chromosomes linearly antagonizes spindle elongation rate, and its correction in anaphase prevents spindle collapse and cell death (Courtheoux *et al.*, 2009). However, quantitative analysis of merotelic attachment and its correction in live cells is poorly documented. MAARS provides a tool to understand the molecular mechanisms of correction.

Quantitative analysis by MAARS of lagging chromosomes has enabled us to detect rare events of correction during anaphase in wild-type and mutant conditions. For example, the presence of merotelic attachment has never been reported in *mod20Δ* cells. Similarly, we were also able to visualize rare events of correction of a missegregated kinetochore in late anaphase in wild-type cells, although it is generally admitted that correction only occurs in metaphase or early anaphase. By following single cells during mitotic progression, it will be possible to identify the timing of correction of merotelic attachment. MAARS will thus be a perfect expert system to decipher the mechanisms of merotelic attachment signaling and correction.

With future developments, MAARS software will deliver high-content information for other mitotic parameters such as kinetochore congression at the metaphase plate or kinetochore oscillation (Mary *et al.*, 2015). A combination analysis of these parameters will create new insights into of mitosis. For example, because mitosis in fission yeast implicates almost 500 proteins, a large-data combinational analysis could unravel new functions for known proteins or assign mitotic functions for unknown proteins. By adapting MAARS's existing segmentation parameters,

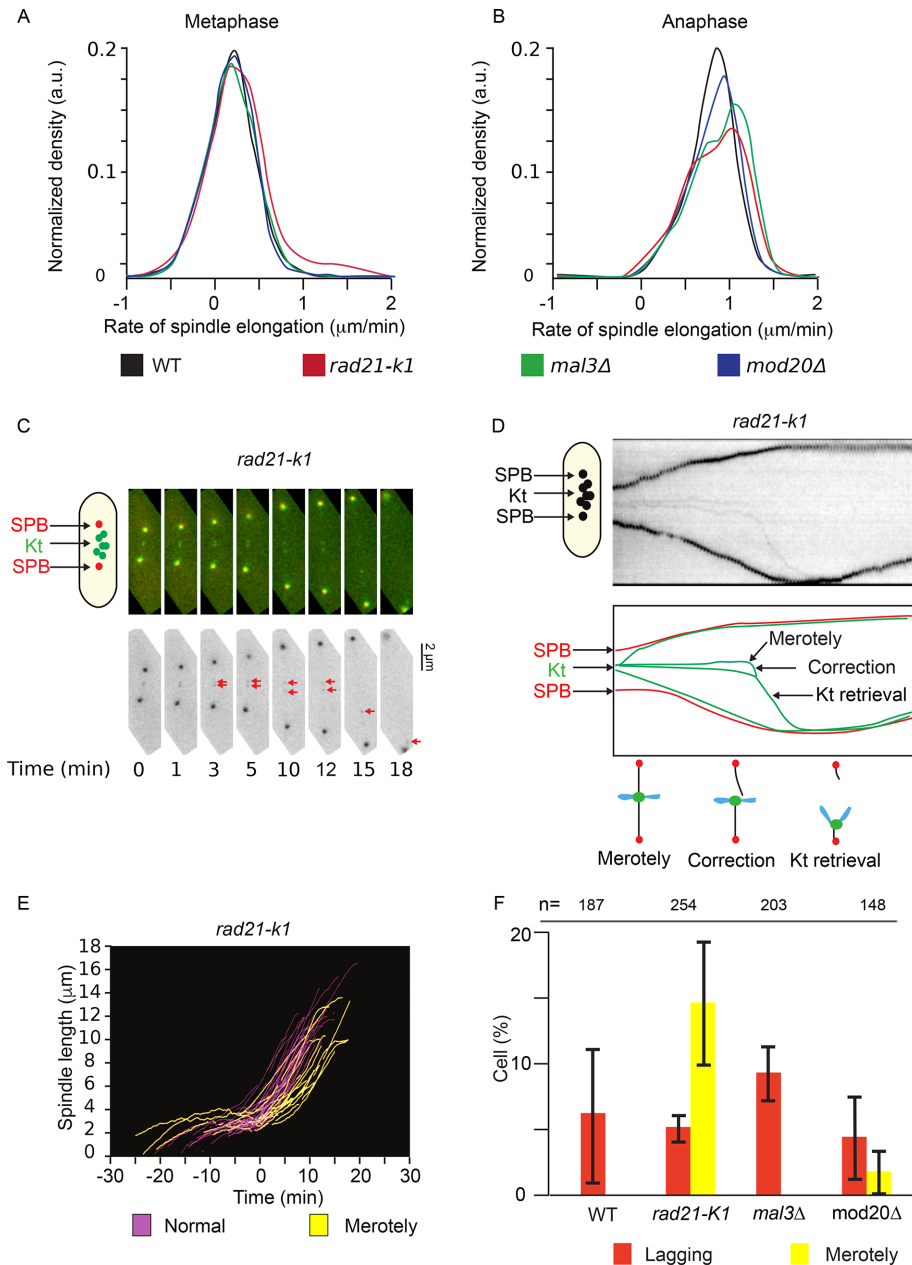


FIGURE 6: Automated detection of lagging kinetochores and merotelic attachment in several genetic backgrounds. (A) Normalized density profiles of spindle elongation speed during metaphase in wild-type (black), *rad21-K1* (red), *mal3Δ* (green), and *mod20Δ* (blue) cells. (B) Normalized density profiles of spindle elongation speed during anaphase B in wild-type (black), *rad21-K1* mutant (red), *mal3Δ* (green), and *mod20Δ* (blue) cells. (C) MAARS automatic detection of merotelic kinetochore correction in *rad21-K1* cells. Red arrows indicate the position of the merotelic kinetochore. (D) Kymograph representation of the correction of the merotelic kinetochore in anaphase. (E) Multiple spindle elongation profiles observed in *rad21-K1* cells ($n = 88$). Spindle elongation profiles in the absence of merotelic attachment are highlighted in pink, and elongation profiles presenting merotelic attachment in anaphase are highlighted in yellow. Time zero corresponds to anaphase onset. (F) Statistical analysis describing the percentages of lagging kinetochores (red) and merotelic kinetochore attachments (yellow) in different cell lines. Error bars correspond to SDs obtained from three independent experiments.

and kinetochore markers as long as a suitable segmentation algorithm is implemented. In conclusion, mitosis research will largely benefit from a quantitative analysis and an expert system approach to understand the ballet of chromosome dynamics in time and space.

open-source license BSD (Berkeley Software Distribution License). Documentation and source code are available in a public repository (<https://github.com/bnoi/MAARS/releases/tag/v1.0.0>). The plug-in as a Jar file can be used in ImageJ. We recommend following

MATERIALS AND METHODS

Cell culture

Media, growth, maintenance of strains, and genetic methods were as reported (Moreno *et al.*, 1991). Cells were grown at 25°C in yeast extract before being mounted on an imaging chamber.

All fluorescently tagged strains (GFP, RFP, and CFP) are integrated at their native chromosomal loci and under the control of their endogenous promoters. The different strains used in this study are listed in Supplemental Table S1.

Cell fixation

To determine the percentage of binucleated and septated cells in *cdc25-22* experiments, cells were fixed in 3.7% formaldehyde for 7 min at room temperature, washed once in phosphate-buffered saline (PBS), and observed in presence of DAPI/calcofluor.

Live-cell imaging

Live-cell microscopy was performed on an imaging chamber (CoverWell PCI-2.5; Grace Bio-Labs) filled with 1 ml of 2% agarose in minimal medium and sealed with a 22 × 22 mm glass coverslip. The temperature was maintained at 25°C during acquisitions. Images were acquired from an inverted wide-field microscope (Nikon Eclipse TI) equipped with a Neo scientific complementary metal oxide semiconductor camera (2560 × 2160 pixel resolution; Andor Technology), an LED light source (Lumencor Spectra), and either a 60× objective (1.40 numerical aperture [NA]) or a 100× objective (1.45 NA).

Mitotic synchronization

The temperature-sensitive mutant *cdc25-22* was synchronized in G2 by incubation at 36°C for 4 h and then released synchronously into mitosis by shifting cells at the permissive temperature of 25°C (>80% of cells were in prometaphase).

Description of MAARS software

MAARS is a Micro-Manager plug-in designed to perform on-the-fly analysis and real-time microscope control or postacquisition analysis. MAARS was written using the Java programming language and uses numerous image-processing libraries, including Fiji (Schindelin *et al.*, 2012), TrackMate (Tinevez *et al.*, 2017), LOCI bioformats (Linkert *et al.*, 2010), and Micro-Manager (Edelstein *et al.*, 2010). MAARS is licensed under

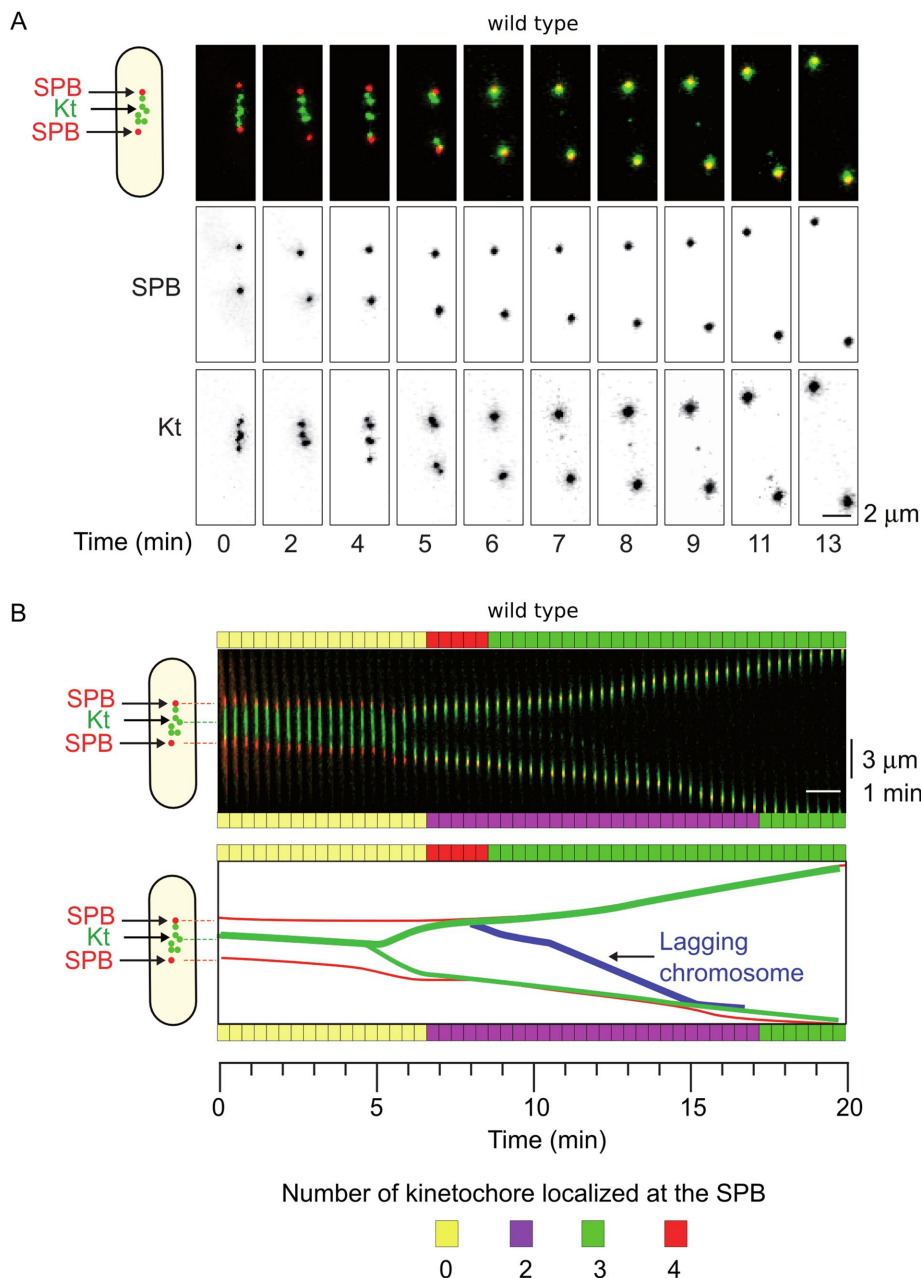


FIGURE 7: Automated detection of rare events of chromosome segregation defects in wild-type cells. (A) Example of a rare event of segregation defect detected by MAARS in a wild-type cell ($n > 8000$ mitotic cells filmed). SPBs in red and kinetochores in green. (B) Top, kymograph representation of the cell shown above. Bottom, automated tracking analysis of the cell shown in A. The number of kinetochores at each SPB is indicated for each time point on both sides of the kymograph; zero (yellow), two (purple), three (green), and four (red). Note the presence of four kinetochores at the upper pole and the correction of the defect during anaphase.

precisely the installation instructions (https://github.com/bnoi/MAARS/blob/master/doc/install_MAARS.md). Several tutorials are also provided (<https://github.com/bnoi/MAARS/tree/master/doc/demos>) to illustrate the simplicity and efficiency of MAARS software.

Bright-field segmentation. Segmentation of *S. pombe* was performed using a correlation imaging technique based on bright-field images taken at various focal positions, as previously described (Julou *et al.*, 2013). The principle of this correlation imaging technique is that under bright-field illumination, the cell wall of

S. pombe changes from a dark to a bright color at various focal positions. This dark-to-bright intensity variation is very similar to the invert derivative of a Gaussian distribution.

We implemented this method to segment fission yeast cells. This segmentation computes a correlation image from a stack of 34 bright-field images taken with a Z-step of 0.3 μ m; 17 images are taken below and the other 17 above the longitudinal axis of the cell. In this three-dimensional stack, every pixel has X-, Y-, and Z-coordinates. For each stack of pixels having the same X- and Y-coordinates, MAARS determines a correlation score between observed and theoretical Gaussian gray value distributions and provides a correlation image transformed in a binary image. Finally, the Particle Analyzer plug-in from Fiji returns polygonal regions of interest (ROIs) as potential “cells.”

Generation of automated ROIs around cells. Previously detected ROIs corresponds to single cells but also to false-positive regions (fused cells, intercell space). Before proceeding to mitotic analysis, MAARS rejects unwanted regions based on decision tree filters such as minimum cell size, maximum cell size, ROI solidity, and ROI mean gray value.

Optimized parallelization. Parallelization in MAARS ensures correct acquisition timing and fast computation. One thread is dedicated to image acquisition, and other threads are allocated for heavy computation such as segmentation or single-cell analysis.

Spot detection. All of the analyses are done in two dimensions after a maximum projection of the stacks. Kinetochores or SPB epitope-tagged strains used in this study appear as bright spots inside cells. MAARS applies a maximum Z-projection of images before spot detection. Then a Laplacian of Gaussian (LoG) detector (from TrackMate Fiji plug-in) detects the spots. To guarantee on-the-fly spot detection with a very low rate of false positives, it is crucial to optimize two parameters: the spot radius and the quality of the spots of interest. Owing to the high variability between biological samples,

multiple parameters, including spot intensity, signal/noise ratio, and so on, could vary slightly. Thus users have to test and modify the parameters of spot detection before launching the MAARS analysis process, by using the test button in the Graphical User Interface. These parameters can be adjusted for each experiment to provide high-quality detection for kinetochores and SPBs.

Mitotic cells and phase detection. The spindle is defined by the recognition of the two SPBs in a single cell. Metrics related to the distance between the two SPBs or their position within the cell can

be easily calculated (e.g., spindle length, spindle orientation). Because the spindle forms in prophase and elongates to reach cell ends in late anaphase B, we determine in each cell the mitotic period as the period of time between the minimum and maximum spindle length as judged by the distance between the SPBs.

A first step in the detection of mitosis consists of finding cells with at least two fluorescent signals (e.g., presence of two spindle poles inside a ROI for a minimum of 3 min). However, fused cells presenting a high solidity value can contaminate this detection. Thus a second step consists of a more precise description of the directed movement of the two spindle poles from prophase to anaphase B (i.e., corresponding to spindle poles moving away from each other during spindle elongation). Although the rate of spindle elongation differs from prophase to anaphase B, we assume that the entire elongation process is roughly linear. Building a model of spindle elongation and finding the best parameters for each strain to detect mitosis is not the optimum way to identify every mitotic cell. Indeed, the detection process may ignore mitotic cells with an abnormal fluorescent signal. In addition, the way in which the spindle elongates may vary from strain to strain. To circumvent this problem, we chose to use a minimum number of parameters to detect mitotic cells by testing the linearity of the elongation curves. For this, we segmented spindle elongation trajectories into a region between the minimum distance between the SPBs and the maximum distance between the SPBs. Then, the program applies a line-fit function on the elongation curve and determines its p value. A threshold of p value resulting in fewer mistakes is used to specifically select mitotic cells. In practice, we chose to use a higher threshold than the optimum p value (i.e., 10^{-11} vs. 10^{-15}) to decrease false-negative detection and accept more false-positive cells, which can be easily eliminated afterward (Supplemental Figure S4). Supplemental Figure S4 shows the total number of errors measured as a function of this threshold.

Virtual cell representation. For the virtual cell representation, the positions of the SPBs are projected into a single virtual cell in order to describe spindle positioning and orientation in a population of cells. However, cells are filmed in random positions, and the coordinates of the cell centers are different. It is thus required to perform both a rotation and a translation of the SPB coordinates. Cell rotation is performed by multiplying all spot coordinates with the corresponding rotation matrix using the angle of the cell major axis. Then cell translation is obtained by subtracting the cell center's coordinates. Thus the reference of each set of cell coordinates is zero.

Determination of slope changes during spindle elongation. Slope changes in the rate of spindle elongation can be used to detect prophase or anaphase B onset. It also can be used to detect the presence of merotelic attachment in anaphase because spindle elongation is reduced in their presence. To locate such changes, we analyze spindle elongation in sliding 3-min windows throughout mitotic progression. Anaphase B onset corresponds to the time point having the maximum slope change among those 3-min windows. This method can also be used to find prophase onset. However, in mutant cells, especially in the case of the *rad21-K1* mutant, for which the slope change at anaphase onset is less brutal, anaphase B onset is determined with less accuracy (± 1 min). In such situations, manually annotating anaphase onset is highly recommended before proceeding to further analysis. Once the annotated elongation curves are aligned according to the onset of anaphase, the program calculates spindle elongation rates before or after this time-point (corresponds to pro/metaphase or anaphase cells). The speed in each phase is shown as a mean value.

Manual annotation. The entire automated detection is not error-free. Thus several semiautomated manual efforts are required. The first type of error is the presence of telophase cells within the analyzed population. Indeed, the two SPBs of cells in telophase can move apart by chance or due to problems of spot detection. Because MAARS saves the cropped images of each cell, the user can get back to the cropped films and reject unwanted telophase cells.

Lagging-chromosome detection. MAARS searches for cells with spots (kinetochores) located between the two spindle poles during anaphase. It confirms an event of anaphase chromosome lagging when a kinetochore between SPBs is detected after anaphase B onset. The corresponding cell appears in a pop-up window at the end of the analysis to allow user confirmation of this event.

ACKNOWLEDGMENTS

We thank the *S. pombe* community for supplying strains, Olivier Gadal (Centre de Biologie Integrative, Toulouse) for supplying a budding yeast strain with SPB markers, Lucie Chadelles for the comments on the MAARS tutorial, and Thomas Mangeat and Guillaume Gay (DamCB, Marseille) for helpful discussions. H.M. was supported by the Fondation pour la Recherche Medicale. J.F. and S.C. were supported by the plan Cancer 2009-2013 Systems Biology. This work was funded by Agence Nationale de la Recherche Blanc120601 Chromocatch and the plan Cancer 2009-2013 Systems Biology. Microscopy equipment was funded by the Centre National de la Recherche Scientifique, Agence Nationale de la Recherche Blanc120601 and l'Association de la Recherche sur le Cancer.

REFERENCES

- Adames NR, Cooper JA (2000). Microtubule interactions with the cell cortex causing nuclear movements in *Saccharomyces cerevisiae*. *J Cell Biol* 149, 863–874.
- Asakawa K, Kume K, Kanai M, Goshima T, Miyahara K, Dhut S, Tee WW, Hirata D, Toda T (2006). The V260I mutation in fission yeast alpha-tubulin *Atb2* affects microtubule dynamics and EB1-Mal3 localization and activates the Bub1 branch of the spindle checkpoint. *Mol Biol Cell* 17, 1421–1435.
- Beinhauer JD, Hagan IM, Hegemann JH, Fleig U (1997). Mal3, the fission yeast homologue of the human APC-interacting protein EB-1 is required for microtubule integrity and the maintenance of cell form. *J Cell Biol* 139, 717–728.
- Carminati JL, Stearns T (1997). Microtubules orient the mitotic spindle in yeast through dynein-dependent interactions with the cell cortex. *J Cell Biol* 138, 629–641.
- Chang F, Nurse P (1993). Finishing the cell cycle: control of mitosis and cytokinesis in fission yeast. *Trends Genet* 9, 333–335.
- Choi SH, McCollum D (2012). A role for metaphase spindle elongation forces in correction of merotelic kinetochore attachments. *Curr Biol* 22, 225–230.
- Cimini D, Cameron LA, Salmon ED (2004). Anaphase spindle mechanics prevent mis-segregation of merotelically oriented chromosomes. *Curr Biol* 14, 2149–2155.
- Cimini D, Wan X, Hirel CB, Salmon ED (2006). Aurora kinase promotes turnover of kinetochore microtubules to reduce chromosome segregation errors. *Curr Biol* 16, 1711–1718.
- Cleveland DW, Mao Y, Sullivan KF (2003). Centromeres and kinetochores: from epigenetics to mitotic checkpoint signaling. *Cell* 112, 407–421.
- Compton DA (2011). Mechanisms of aneuploidy. *Curr Opin Cell Biol* 23, 109–113.
- Conrad C, Wunsche A, Tan TH, Bulkescher J, Sieckmann F, Verissimo F, Edelstein A, Walter T, Liebel U, Pepperkok R, Ellenberg J (2011). Micro-pilot: automation of fluorescence microscopy-based imaging for systems biology. *Nat Methods* 8, 246–249.
- Courteoux T, Gay G, Gachet Y, Tournier S (2009). Ase1/Prc1-dependent spindle elongation corrects merotelically attached chromosomes during anaphase in fission yeast. *J Cell Biol* 187, 399–412.

- Edelstein A, Amodaj N, Hoover K, Vale R, Stuurman N (2010). Computer control of microscopes using microManager. *Curr Protoc Mol Biol* Chapter 14, Unit 14.20.
- Franco A, Meadows JC, Millar JB (2007). The Dam1/DASH complex is required for the retrieval of unclustered kinetochores in fission yeast. *J Cell Sci* 120, 3345–3351.
- Gachet Y, Reyes C, Courthoux T, Goldstone S, Gay G, Serrurier C, Tournier S (2008). Sister kinetochore recapture in fission yeast occurs by two distinct mechanisms, both requiring Dam1 and Klp2. *Mol Biol Cell* 19, 1646–1662.
- Gachet Y, Tournier S, Millar JB, Hyams JS (2004). Mechanism controlling perpendicular alignment of the spindle to the axis of cell division in fission yeast. *EMBO J* 23, 1289–1300.
- Gao Q, Courthoux T, Gachet Y, Tournier S, He X (2010). A non-ring-like form of the Dam1 complex modulates microtubule dynamics in fission yeast. *Proc Natl Acad Sci USA* 107, 13330–13335.
- Gay G, Courthoux T, Reyes C, Tournier S, Gachet Y (2012). A stochastic model of kinetochore-microtubule attachment accurately describes fission yeast chromosome segregation. *J Cell Biol* 196, 757–774.
- Gregan J, Riedel CG, Pidoux AL, Katou Y, Rumpf C, Schleiffer A, Kearsey SE, Shirahige K, Allshire RC, Nasmyth K (2007). The kinetochore proteins Pcs1 and Mde4 and heterochromatin are required to prevent merotelic orientation. *Curr Biol* 17, 1190–1200.
- Grishchuk EL, McIntosh JR (2006). Microtubule depolymerization can drive poleward chromosome motion in fission yeast. *EMBO J* 25, 4888–4896.
- Holland AJ, Cleveland DW (2009). Boveri revisited: chromosomal instability, aneuploidy and tumorigenesis. *Nat Rev Mol Cell Biol* 10, 478–487.
- Julou T, Mora T, Guillon L, Croquette V, Schalk IJ, Bensimon D, Desprat N (2013). Cell-cell contacts confine public goods diffusion inside *Pseudomonas aeruginosa* clonal microcolonies. *Proc Natl Acad Sci USA* 110, 12577–12582.
- Kalinina I, Nandi A, Delivani P, Chacon MR, Klemm AH, Ramunno-Johnson D, Krull A, Lindner B, Pavin N, Tolic-Norrelykke IM (2013). Pivoting of microtubules around the spindle pole accelerates kinetochore capture. *Nat Cell Biol* 15, 82–87.
- Kirschner M, Mitchison T (1986). Beyond self-assembly: from microtubules to morphogenesis. *Cell* 45, 329–342.
- Kohli J, Hottinger H, Munz P, Strauss A, Thuriaux P (1977). Genetic mapping in *Schizosaccharomyces pombe* by mitotic and meiotic analysis and induced haploidization. *Genetics* 87, 471–489.
- Kotak S, Gonczy P (2013). Mechanisms of spindle positioning: cortical force generators in the limelight. *Curr Opin Cell Biol* 25, 741–748.
- Kotwaliwal CV, Frei SB, Stern BM, Biggins S (2007). A pathway containing the Ipl1/aurora protein kinase and the spindle midzone protein Ase1 regulates yeast spindle assembly. *Dev Cell* 13, 433–445.
- Kozlowski C, Srayko M, Nedelec F (2007). Cortical microtubule contacts position the *C. elegans* embryos. *Cell* 129, 499–510.
- Linkert M, Rueden CT, Allan C, Burel JM, Moore W, Patterson A, Loranger B, Moore J, Neves C, Macdonald D, et al. (2010). Metadata matters: access to image data in the real world. *J Cell Biol* 189, 777–782.
- Mary H, Fouchard J, Gay G, Reyes C, Gauthier T, Gruget C, Pecreaux J, Tournier S, Gachet Y (2015). Fission yeast Kinesin-8 controls chromosome congression independently of oscillations. *J Cell Sci* 128, 3720–3730.
- Mora-Bermudez F, Gerlich D, Ellenberg J (2007). Maximal chromosome compaction occurs by axial shortening in anaphase and depends on Aurora kinase. *Nat Cell Biol* 9, 822–831.
- Moreno S, Klar A, Nurse P (1991). Molecular genetic analysis of fission yeast *Schizosaccharomyces pombe*. *Methods Enzymol* 194, 795–823.
- Nabeshima K, Nakagawa T, Straight AF, Murray A, Chikashige Y, Yamashita YM, Hiraoka Y, Yanagida M (1998). Dynamics of centromeres during metaphase-anaphase transition in fission yeast: Dis1 is implicated in force balance in metaphase bipolar spindle. *Mol Biol Cell* 9, 3211–3225.
- Niwa O (2016). Determination of the frequency of minichromosome loss to assess chromosome stability in fission yeast. *Cold Spring Harb Protoc* 2016(Jun 24), doi: 10.1101/pdb.prot091991.
- Nurse P (1975). Genetic control of cell size at cell division in yeast. *Nature* 256, 547–551.
- Nurse P, Thuriaux P (1980). Regulatory genes controlling mitosis in the fission yeast *Schizosaccharomyces pombe*. *Genetics* 96, 627–637.
- Page BD, Snyder M (1993). Chromosome segregation in yeast. *Annu Rev Microbiol* 47, 231–261.
- Peng JY, Chen YJ, Green MD, Sabatinos SA, Forsburg SL, Hsu CN (2013). PombeX: robust cell segmentation for fission yeast transillumination images. *PLoS One* 8, e81434.
- Petersen J, Hagan IM (2003). *S. pombe* aurora kinase/survivin is required for chromosome condensation and the spindle checkpoint attachment response. *Curr Biol* 13, 590–597.
- Petersen J, Paris J, Willer M, Philippe M, Hagan IM (2001). The *S. pombe* aurora-related kinase Ark1 associates with mitotic structures in a stage dependent manner and is required for chromosome segregation. *J Cell Sci* 114, 4371–4384.
- Rieder CL, Cole RW, Khodjakov A, Sluder G (1995). The checkpoint delaying anaphase in response to chromosome monoorientation is mediated by an inhibitory signal produced by unattached kinetochores. *J Cell Biol* 130, 941–948.
- Rudner AD, Murray AW (1996). The spindle assembly checkpoint. *Curr Opin Cell Biol* 8, 773–780.
- Rumpf C, Cipak L, Schleiffer A, Pidoux A, Mechtler K, Tolic-Norrelykke IM, Gregan J (2010). Laser microsurgery provides evidence for merotelic kinetochore attachments in fission yeast cells lacking Pcs1 or Clr4. *Cell Cycle* 9, 3997–4004.
- Russell P, Moreno S, Reed SI (1989). Conservation of mitotic controls in fission and budding yeasts. *Cell* 57, 295–303.
- Sampath SC, Ohi R, Leismann O, Salic A, Pozniakovski A, Funabiki H (2004). The chromosomal passenger complex is required for chromatin-induced microtubule stabilization and spindle assembly. *Cell* 118, 187–202.
- Sawin KE, Lourenco PC, Snaith HA (2004). Microtubule nucleation at non-spindle pole body microtubule-organizing centers requires fission yeast centrosomin-related protein mod20p. *Curr Biol* 14, 763–775.
- Schindelin J, Arganda-Carreras I, Frise E, Kaynig V, Longair M, Pietzsch T, Preibisch S, Rueden C, Saalfeld S, Schmid B, et al. (2012). Fiji: an open-source platform for biological-image analysis. *Nat Methods* 9, 676–682.
- Schmitter D, Wachowicz P, Sage D, Chasapi A, Xenarios I, Simanis, Unser M (2013). A 2D/3D image analysis system to track fluorescently labeled structures in rod-shaped cells: application to measure spindle pole asymmetry during mitosis. *Cell Div* 8, 6.
- Segal M, Bloom K (2001). Control of spindle polarity and orientation in *Saccharomyces cerevisiae*. *Trends Cell Biol* 11, 160–166.
- Shaw SL, Yeh E, Maddox P, Salmon ED, Bloom K (1997). Astral microtubule dynamics in yeast: a microtubule-based searching mechanism for spindle orientation and nuclear migration into the bud. *J Cell Biol* 139, 985–994.
- Steigemann P, Wurzenberger C, Schmitz MH, Held M, Guizetti J, Maar S, Gerlich DW (2009). Aurora B-mediated abscission checkpoint protects against tetraploidization. *Cell* 136, 473–484.
- Tada K, Susumu H, Sakuno T, Watanabe Y (2011). Condensin association with histone H2A shapes mitotic chromosomes. *Nature* 474, 477–483.
- Tanaka TU, Rachidi N, Janke C, Pereira G, Galova M, Schiebel E, Stark MJ, Nasmyth K (2002). Evidence that the Ipl1-Sli15 (Aurora kinase-INCENP) complex promotes chromosome bi-orientation by altering kinetochore-spindle pole connections. *Cell* 108, 317–329.
- Tatebe H, Goshima G, Takeda K, Nakagawa T, Kinoshita K, Yanagida M (2001). Fission yeast living mitosis visualized by GFP-tagged gene products. *Micron* 32, 67–74.
- Tinevez JY, Perry N, Schindelin J, Hoopes GM, Reynolds GD, Laplantine E, Bednarek SY, Shorte SL, Eliceiri KW (2017). TrackMate: an open and extensible platform for single-particle tracking. *Methods* 115, 80–90.
- Tournier S, Gachet Y, Buck V, Hyams JS, Millar JB (2004). Disruption of astral microtubule contact with the cell cortex activates a Bub1, Bub3, and Mad3-dependent checkpoint in fission yeast. *Mol Biol Cell* 15, 3345–3356.
- Tran PT, Marsh L, Doye V, Inoue S, Chang F (2001). A mechanism for nuclear positioning in fission yeast based on microtubule pushing. *J Cell Biol* 153, 397–411.
- Vardy L, Toda T (2000). The fission yeast gamma-tubulin complex is required in G(1) phase and is a component of the spindle assembly checkpoint. *EMBO J* 19, 6098–6111.
- Venkatram S, Jennings JL, Link A, Gould KL (2005). Mto2p, a novel fission yeast protein required for cytoplasmic microtubule organization and anchoring of the cytokinetic actin ring. *Mol Biol Cell* 16, 3052–3063.
- Vitre BD, Cleveland DW (2012). Centrosomes, chromosome instability (CIN) and aneuploidy. *Curr Opin Cell Biol* 24, 809–815.
- Yanagida M (1998). Fission yeast cut mutations revisited: control of anaphase. *Trends Cell Biol* 8, 144–149.
- Yanagida M (2000). Cell cycle mechanisms of sister chromatid separation; roles of Cut1/separin and Cut2/securin. *Genes Cells* 5, 1–8.
- Yeh E, Yang C, Chin E, Maddox P, Salmon ED, Lew DJ, Bloom K (2000). Dynamic positioning of mitotic spindles in yeast: role of microtubule motors and cortical determinants. *Mol Biol Cell* 11, 3949–3961.
- Zimmerman S, Chang F (2005). Effects of {gamma}-tubulin complex proteins on microtubule nucleation and catastrophe in fission yeast. *Mol Biol Cell* 16, 2719–2733.